Effects of Preview Time in Manual Tracking Tasks

El, Kasper van der; Padmos, Sharon; Pool, Daan M.; van Paassen, Marinus M.; Mulder, Max

DOI
10.1109/THMS.2018.2834871

Publication date
2018

Document Version
Accepted author manuscript

Published in
IEEE Transactions on Human-Machine Systems

Citation (APA)
El, K. V. D., Padmos, S., Pool, D. M., van Paassen, M. M., & Mulder, M. (2018). Effects of Preview Time in Manual Tracking Tasks. *IEEE Transactions on Human-Machine Systems*, *48*(5), 486 - 495. https://doi.org/10.1109/THMS.2018.2834871

Effects of Preview Time in Manual Tracking Tasks

Kasper van der El, *Student Member, IEEE,* Sharon Padmos, Daan M. Pool, *Member, IEEE,* Marinus (René) M. van Paassen, *Senior Member, IEEE,* and Max Mulder, *Member, IEEE*

***Abstract*—In manual control tasks, preview of the target trajectory ahead is often limited by poor lighting, objects, or display edges. This paper investigates the effects of limited preview, or preview time, in manual tracking tasks with single- and double-integrator controlled element dynamics. A quasi-linear human controller model is used to predict human behavior adaptations offline, by finding the model parameters that yield optimal performance at each preview time. These predictions are then verified by fitting the same model to measurements from a human-in-the-loop experiment, where subjects performed a tracking task with eight different preview time settings between 0 and 2 s. Results show that tracking performance improves and that the model's "look-ahead" time parameters increase with increasing preview time. Beyond a certain preview time, approximately 0.6 and 1.15 s in single- and double-integrator tasks, respectively, additional preview evokes no further adaptations. The offline model predictions closely match the experimental results, which thereby promises to facilitate similar quantitative insights in other tasks with restricted preview.**

***Index Terms*—Manual control, modeling, parameter estimation, preview time, system identification**

I. Introduction

PREVIEW information about a future trajectory to follow is present in many manual control tasks. A clear example of preview is the road that is visible ahead when driving [1]. The extent of the visible preview is always limited by the horizon, fog, poor lighting, objects, or display edges. The "preview time" is the time required to reach the farthest visible point on the previewed trajectory at the current velocity. It has been shown that Human Controllers (HCs) can better follow a target trajectory when the preview time increases, in tasks ranging from display tracking [2]–[7] to car driving [8]–[11]. However, task performance is typically stable when the preview time exceeds a certain minimum, or "critical" preview time, which is known to range between 0.3-1.5 s, depending on the control task [3]–[6], [8]. To assure safe manual operation in control tasks with restricted preview, it is essential to quantify and, if possible, predict the critical preview time and the performance degradation at lower preview times.

The effects of preview time on HC behavior are as of yet not fully understood. Task characteristics (or variables) such as the Controlled Element (CE) dynamics and target trajectory bandwidth also evoke HC behavior adaptations [12], [13], and influence the effects of preview, including the critical time [5], [14]. Attempts to quantify the effects of preview time through control-theoretic modeling of driver steering [1], [15]–[18] and manual tracking [2], [3], [5], [19] account for HCs' use of preview in fundamentally different ways. We recently proposed a new quasi-linear model for preview tracking tasks [19], which captures measured HC multiloop control dynamics in tracking tasks with 0 s (pursuit) and 1 s of preview. Preliminary experimental results suggest that this model can also capture HC adaptation to preview time [7], but this was only shown for rate control tasks with preview times between 0 and 1 s. The model's physically interpretable parameters can be directly estimated from experimental data using system identification, yielding novel quantitative insights into how HCs use preview. This already led to an initial set of "verbal adjustment rules" that cover HC adaptation to the CE dynamics in preview tracking tasks [14]. Unfortunately, we currently lack the understanding and experimental data that are required to formulate similar rules for the effects of other task variables, such as available preview time [13].

The goal of this paper is to quantify the effects of preview time in manual tracking tasks; in particular, we investigate the critical preview time and changes in task performance and HC control behavior. As the CE dynamics are known to strongly affect HCs' use of preview [14], we investigate the effects of preview time with both Single Integrator (SI, rate control) and Double Integrator (DI, acceleration control) CE dynamics.

We will first use the quasi-linear preview model from [19] to theoretically predict the effects of preview time offline, by finding the model parameters (i.e., the HC's behavior) that minimize the tracking error in closed-loop model simulations. Second, we verify these predictions with measurements from a human-in-the-loop experiment, in which eight subjects performed the same target-tracking and disturbance-rejection task, with eight different preview times between 0 and 2 s (well above reported critical preview times [3]–[6], [8]). To explicitly quantify HCs' adaptation to preview time, we apply a nonparametric, multiloop system identification technique [20], and we make a least-squares fit of the preview model to the measurement data to estimate the model's parameters.

This paper is structured as follows. First, Section II introduces the considered preview tracking task and the preview control model from [19]. Predictions of the effects of preview time are presented in Section III, followed by the experimental method and the applied identification techniques in Section IV. Section V summarizes the experiment results and compares them to the predictions. The paper ends with a discussion and our main conclusions in Sections VI and VII, respectively.

II. The Control Task

Fig. 1 illustrates the considered control task and shows the principal terminology used throughout this paper. The HC's

Manuscript submitted August 23, 2017; revised December 29, 2017 and April 9, 2018. Corresponding author: Kasper van der El.

The authors are with the Control and Simulation section, Faculty of Aerospace Engineering, Delft University of Technology, 2629 HS Delft, The Netherlands (e-mail: k.vanderel@tudelft.nl).

Digital Object Identifier: 10.1109/THMS.2018.2834871.

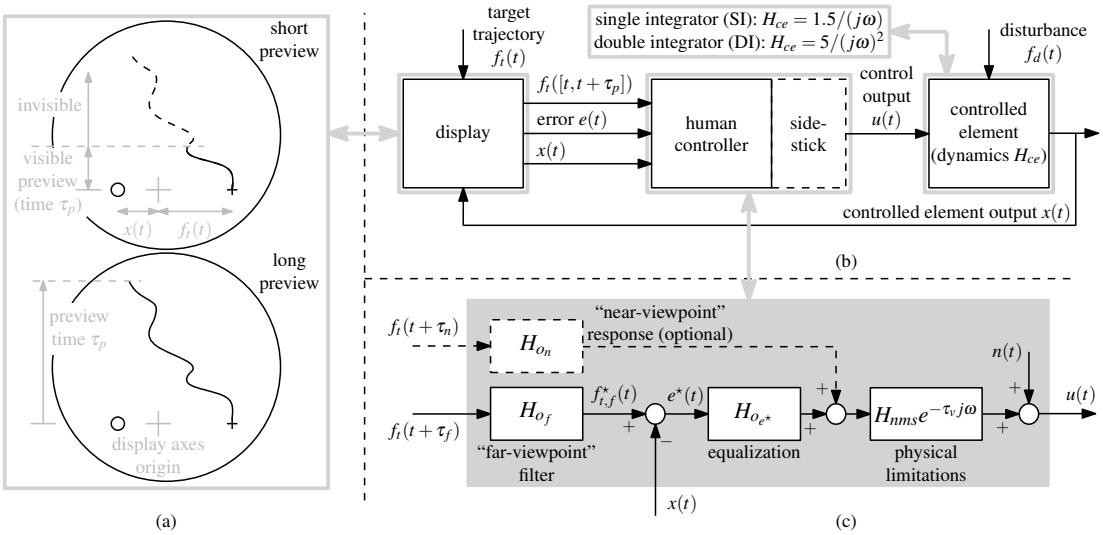

Fig. 1. Preview displays with different preview times (a), illustration of the control task (b), and the model for HC preview tracking behavior from [19] (c).

task is to give control inputs $u(t)$ to the CE such that the CE output $x(t)$ (white circle on the display, Fig. 1a) horizontally follows the target signal $f_t(t)$ (black cross) as closely as possible, while the CE output is simultaneously perturbed by a disturbance signal $f_d(t)$. In other words, the HC should minimize the horizontal tracking error $e(t)=f_t(t)-x(t)$. On the displays (Fig. 1a) the target signal $f_t([t,t+\tau_p])$ ahead is also visible (winding line) up to the preview time τ_p s ahead. The previewed target signal can be used by the HC to anticipate the future horizontal movements of the current target marker. When τ_p is zero, only the current target is visible and a classical pursuit task is obtained [10].

The model of HC behavior in preview tracking tasks from [19] is depicted in Fig. 1c. The model is quasi-linear, with linear time-invariant transfer functions $H(j\omega)$ that account for the majority of the HC's behavior, and a remnant signal $n(t)$ that captures the remaining time-variations, nonlinearities, and noise. HC use of the full previewed target is modeled with two responses. The main, low-frequency, "far-viewpoint" response allows for most performance improvement relative to zero-preview, pursuit tasks, while the auxiliary, high-frequency, "near-viewpoint" response improves performance slightly more at a cost of a substantial increase in control effort [14]. The far-viewpoint response involves an identical feedback control-strategy as in compensatory tracking tasks [12]; however, the error $e^\star(t)$ that is minimized is not the true error $e(t)$, but the difference between the filtered target at the far viewpoint τ_f s ahead and the CE output: $E^\star(j\omega) = H_{o_f}(j\omega)e^{\tau_f j\omega}F_t(j\omega) - X(j\omega)$, with the capital letters denoting the Fourier transforms of the respective signals. The low-pass smoothing filter $H_{o_f}(j\omega)$ is given by:

$$H_{o_f}(j\omega) = K_f \frac{1}{1+T_{l,f}j\omega}, \tag{1}$$

with target weighting gain K_f and time constant $T_{l,f}$. HCs completely ignore the target signal variations when K_f=0, while K_f=1 indicates a response to the true advanced error, at least at those frequencies sufficiently below the smoothing filter cutoff $1/T_{l,f}$ [14]. In the time domain, the low-pass filter in (1) can be interpreted as the weighted average of the previewed target up to the far viewpoint, such that τ_f is the most distance point on the previewed trajectory that is used by the HC, while $T_{l,f}$ quantifies the portion of the visible preview that is used for smoothin the trajectory.

The modeled error response $H_{o_{e^\star}}(j\omega)$ is a reduced form of McRuer *et al.*'s precision model [21]:

$$H_{o_{e^\star}}(j\omega) = K_{e^\star}(1+T_{L,e^\star}j\omega). \tag{2}$$

Here, $K_{e^\star}$ is the error response gain and $T_{L,e^\star}$ is the lead time constant. Possible lag equalization is omitted in (2), as such behavior is normally absent in SI and DI tasks [12]. In SI tasks no lead equalization is required and (2) reduces to $K_{e^\star}$[1]. The HC's physical limitations are also included in this inner loop: τ_v is the response time delay and $H_{nms}(j\omega)$ represents the neuromuscular activation dynamics [23], modeled here as a second-order mass-spring-damper system [19],

$$H_{nms}(j\omega) = \frac{\omega_{nms}^2}{(j\omega)^2 + 2\zeta_{nms}\omega_{nms}j\omega + \omega_{nms}^2}, \tag{3}$$

with a break frequency ω_{nms} and damping ratio ζ_{nms}.

The open-loop, near-viewpoint response $H_{o_n}(j\omega)$, although not always initiated by all HCs, is used in parallel with the far-viewpoint response to better track the highest frequencies of the target signal [14], [19]. Whether HCs apply a near-viewpoint response likely depends on their motivation to attain optimal performance (it requires substantial effort [14]), and familiarity with the task's CE dynamics and target signal, which is essential for applying an open-loop feedforward control strategy effectively. Longer preview times may trigger the near-viewpoint response, as the HC's knowledge of the target signal improves. With 1 s of preview, most subjects were found to apply a near-viewpoint response in SI tasks, but not in DI

[1]Note that preview tasks with SI dynamics may evoke some low-frequency lag-lead behavior [22]; as this behavior was absent in our experiment, the lag-lead dynamics are excluded from the SI model in this paper.

tasks [14], as accurate feedforward control with these unstable dynamics is difficult [24], [25]. Although not all subtleties of the near-viewpoint response are yet understood, its dynamics appear to approximate a simple differentiator [14]:

$$H_{o_n}(j\omega) = K_n j\omega, \tag{4}$$

with gain K_n, and the target τ_n s ahead as the input. In the following, we will analyze two models: the "Full Model" (FM) with parameter vector $\Theta = [K_n\ \tau_n\ K_f\ T_{l,f}\ \tau_f\ K_{e^\star}\ T_{L,e^\star}\ \omega_{nms}\ \zeta_{nms}\ \tau_v]^T$, as well as a "Reduced Model" (RM) that omits the near-viewpoint response (i.e., no K_n and τ_n).

III. Offline Model Predictions

In this section, we use the preview model from [19] to predict the effects of preview time on HC behavior and tracking performance. Two scenarios are investigated: a Reduced Model Prediction (RMP) and a Full Model Prediction (FMP), obtained with the RM ($H_{o_n}(j\omega)$=0) and FM ($H_{o_n}(j\omega)$ is used) versions of the model, respectively.

A. Approach

Humans are known to be adaptive controllers that optimize their control gains [12], [16], [26], [27]. This adaptation can be expressed mathematically with an optimality criterion that reflects the HC's goals, like a weighted combination of optimized performance and minimized control effort. Motivated HCs typically aim mainly for optimal tracking performance [12], [26], so a good prediction of the model parameter vector Θ is obtained by minimizing the variance of the error, $\sigma_e^2(\Theta)$. The variance can be calculated in the frequency domain by integrating the power spectral density function of the error signal [28].

To calculate the tracking error, we first lump the modeled HC dynamics from the previous section into two describing functions $H_{o_t}(j\omega)$ and $H_{o_x}(j\omega)$, which represent the HC's total response to the target and CE output signals (see Fig. 2 for the corresponding equivalent control diagram [14], [19]):

$$H_{o_x} = H_{o_{e^\star}} H_{nms} e^{-\tau_v j\omega}, \tag{5}$$

$$H_{o_t} = [H_{o_n} e^{\tau_n j\omega} + H_{o_f} e^{\tau_f j\omega} H_{o_{e^\star}}] H_{nms} e^{-\tau_v j\omega} \tag{6}$$

Here, the $j\omega$ terms are dropped for brevity. Expressing $X(j\omega)$ as a function of the external inputs $F_t(j\omega)$, $F_d(j\omega)$, and $N(j\omega)$ using Fig. 2, and substituting the result into $E(j\omega)$=$F_t(j\omega)$−$X(j\omega)$, yields for the tracking error [29]:

$$E = \frac{(1 + H_{ce}(H_{o_x} - H_{o_t}))F_t - F_d - H_{ce}N}{1 + H_{o_x}H_{ce}}. \tag{7}$$

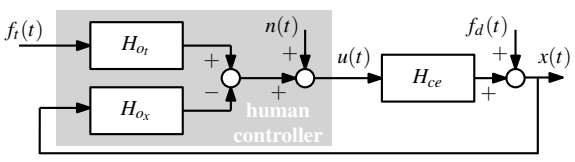

Fig. 2. Two-channel equivalent control diagram of the HC.

B. Settings and Procedure

HC adaptation to variations in τ_p between 0 and 2 s is predicted by minimizing $\sigma_e^2(\Theta)$, subject to a minimum phase margin constraint of 20 deg. The preview time is varied with a 0.01 s resolution, and at each preview time the near- and far-viewpoint locations are constrained to the visible preview region, that is $0 \le \tau_n \le \tau_p$ and $0 \le \tau_f \le \tau_p$. The human's limitation parameters and lead time constant are kept fixed, their values are based on the preview tracking data in [14] (see Table I). For the RMP, the error variance is optimized for the remaining four model parameters: $K_{e^\star}$, K_f, τ_f, and $T_{l,f}$. For the FMP, the error variance is optimized for K_n, τ_n, and $T_{l,f}$, while $K_{e^\star}$, K_f, and τ_f are fixed at the optimal values found in the RMP, as their interaction with the desired near-viewpoint response is small [14]. However, $T_{l,f}$ is again free to allow for an attenuated far-viewpoint response at high frequencies, which may improve the effectiveness of the near-viewpoint response. The predicted performance is compared to human-in-the-loop data from previous experiments for verification, see Table II.

The target signal is a multisine composed of 20 sinusoids:

$$f_t(t) = \sum_{i=1}^{20} A_t[i] \sin(\omega_t[i]t + \phi_t[i]), \tag{8}$$

with amplitude $A_t[i]$, frequency $\omega_t[i]$, and phase $\phi_t[i]$ of the i^{th} sinusoid. The disturbance signal is defined identically, whereas remnant is set to zero. The target and disturbance signals have mutually exclusive frequencies, which are distributed logarithmically between 0.1 and 16 rad/s at integer multiples of the 0.0524 rad/s (=2π/120) fundamental frequency, corresponding to a 120 s measurement time. Both signals have a square amplitude spectrum, with a 1.5 rad/s bandwidth beyond which the amplitudes are attenuated. The variance of the target $\sigma_{f_t}^2$ and disturbance $\sigma_{f_d}^2$ signal is 1.61 cm^2 and 0.26 cm^2, respectively. Both signals are identical to those used in [14], [19], see [19] for the exact values of A_t, ω_t, and ϕ_t.

C. Results

Fig. 3 shows that both the RMP and FMP predict an improved tracking performance with increasing preview time

TABLE I
Offline Model Simulations Parameter Settings.

	$H_{ce}(j\omega)$	$T_{L,e^\star}$, s	ω_{nms}, rad/s	ζ_{nms}, -	τ_v, s
SI	$1.5/(j\omega)$	-	10.5	0.35	0.26
DI	$5/(j\omega)^2$	1.5	8	0.45	0.3

TABLE II
Previous Preview Tracking Experiments.

	CE	dist. added	forcing function	bandwidth, rad/s	no. subj.
Reid [3]	SI	no	filt. noise	-	6
Ito [4]	SI, DI	no	multisine	2.5	2
Tomizuka [5]	SI, DI	no	filt. noise	1.5	3
Van der El [7]	SI	yes	multisine	1.5	6

τ_p, as the normalized error variance $\sigma_e^2/(\sigma_{f_t}^2+\sigma_{f_d}^2)$ decreases. In SI and DI tasks the RMP predicts that optimal performance is reached with approximately 0.6 and 1.15 s of preview, respectively. Additional preview beyond this critical preview time is not necessary for optimal performance, hence invariant HC behavior is predicted (the gray areas in Fig. 3). Below the critical preview time (white areas), HCs can benefit from additional preview by adapting their control behavior. The FMP predicts that a near-viewpoint response can considerably reduce the critical preview time. However, actual HCs can likely initiate this open-loop feedforward response only at higher preview times, when full periods of the high-frequency target sinusoids' are explicitly visible within τ_p [14].

Fig. 3 shows that various previous human-in-the-loop experiments [3], [5], [7] indeed measured optimal performance around our predicted critical preview time, both in SI and DI tasks. Only Ito & Ito [4] found a somewhat lower critical preview time, which may be due to the higher bandwidth of their target signal (2.5 rad/s, see Table II). The predicted performance variations with preview time are also similar to the previous measurements [3]–[5], [7]. However, our current model predictions generally yield better overall performance, as no remnant is included.

The RMP shows that a large performance benefit is possible by only adapting the far-viewpoint response. In particular, it is beneficial to keep the far viewpoint located at the endpoint of the previewed target signal (i.e., $\tau_f{=}\tau_p$ in Fig. 3) when more preview becomes available below the critical preview time. Moreover, $T_{l,f}$ increases in DI tasks, such that more of the high frequencies are cognitively filtered from the target signal with additional preview, as a longer portion of the trajectory is used for smoothing. Predicted adaptations of the other RMP parameters, $K_{e^\star}$ and K_f, are presented together with the experimental measurements in Section V.

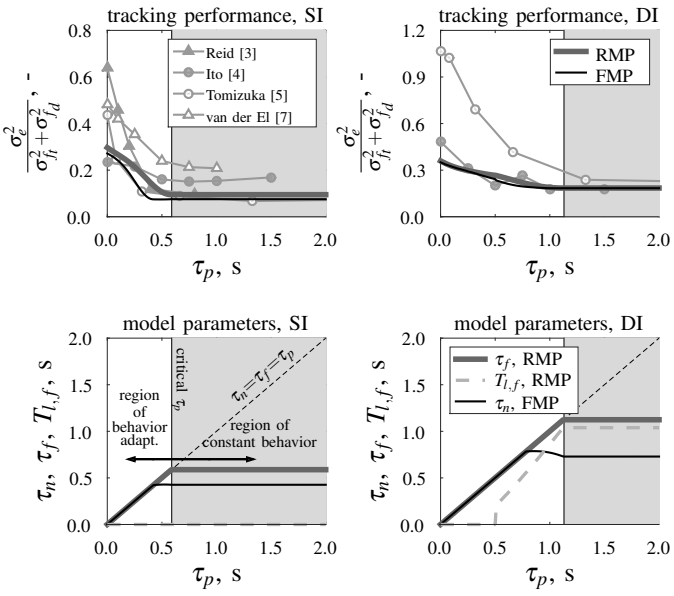

Fig. 3. Predicted tracking performance as compared to previous experiments (top), and the optimal model parameters (bottom); the transition to the shaded region indicates the predicted critical preview time.

The FMP shows that, at short preview times, the near viewpoint's ideal position is also at the endpoint of the previewed target (i.e., $\tau_n{=}\tau_f{=}\tau_p$ in Fig. 3). This indicates a single-viewpoint control strategy, as the near- and far-viewpoint responses are based on the same point on the target ahead. However, as explained before, it is unlikely that actual HCs initiate a near-viewpoint response at low preview times. At higher preview times (but still below the critical preview time), τ_n is predicted to be smaller than τ_f, which suggests that a two-viewpoint control strategy can yield improved performance. In this preview region it is more likely that actual HCs apply a near-viewpoint response, because there is additional preview beyond τ_n that can be used to plan this open-loop feedforward control. As shown before [14], only a marginal performance improvement can be achieved relative to a far-viewpoint control strategy only. With sufficient preview, the optimal near-viewpoint position is around 0.4 and 0.7 s ahead in SI and DI tasks, respectively.

IV. Experimental Validation: Method

The predicted effects of varying preview time are verified with a human-in-the-loop experiment. Details of this experiment are presented here, together with the system identification techniques applied to analyze the measurements.

A. Hypotheses

We expect that the offline model predictions, which assume that HCs aim only for optimal performance, accurately reflect actual HC control adaptation to preview time. This leads to the following three hypotheses:

- I: Below the critical preview time, HCs adapt their control behavior (characterized by estimated preview model parameters) to increasing preview time to improve tracking performance. Most importantly, they position their far-viewpoint as far ahead as possible ($\tau_f{\approx}\tau_p$).
- II: Beyond the critical preview time, HC behavior and tracking performance are invariant with preview time.
- III: The critical preview times in SI and DI tasks are 0.6 s and 1.15 s, respectively.

We formulate no hypothesis about the near-viewpoint response, because its possible contribution is only small (see Section III), and, in addition, previous work has shown that it is often difficult to consistently detect the near-viewpoint's presence from experimental data [14].

B. Experiment Design

1) Independent Variables: In the experiment, we tested eight preview times between 0 and 2 s, in both SI and DI tasks (their dynamics were equal as in the offline analysis). The tested preview times included 0 and 1 s to allow for direct comparison with earlier data [14], [19], preview times of 0.25, 0.5 and 0.75 s were added in-between for a sufficient resolution in the predicted "region of behavior adaption" (see Fig. 3). In addition, preview times of 1.33, 1.66 and 2 s

were included to also ensure sufficient data in the "region of constant behavior". The full factorial of the two independent variables was tested, yielding 16 conditions in total.

2) Control Variables and Apparatus: The experiment was conducted in the fixed-base simulator in the Human-Machine Interaction Laboratory at TU Delft. The setup was identical to the preview tracking experiment in [19]. Subjects were seated directly in front of the screen on which the preview display of Fig. 1 was shown with dark green lines and indicators on a black background. Subjects gave control inputs with a side-stick at their right-hand side (0.45 cm/deg input scaling), which was configured to only rotate around its roll axis. The target and disturbance forcing functions were also identical to those used in [19]. Five different phase realizations of the target signal were used to prevent subjects from recognizing parts after repeated exposure.

3) Participants, Instructions, and Procedure: Eight male volunteers participated in the experiment. They were aged between 23 and 54, with an average of 32 years, and their tracking experience ranged from novice to experienced. Subjects were instructed to minimize the tracking error, and the RMS value of this error was reported to the subjects after every run to motivate them to keep improving their performance.

To reduce effects of fatigue, the experiment was divided over two sessions, which took place on different days. Half of the subjects performed the SI conditions first, while the other half of the subjects performed the DI conditions first. The eight different preview times for each CE were performed in a single session. The conditions were presented to the subjects in a random order following a Latin-square design. Before starting each experimental session, subjects could familiarize themselves with the CE and all eight preview times, each being presented once in descending order from 2 to 0 s. Next, the subjects performed a single condition until at least 8 runs were completed and performance was stable in the last five consecutive runs, which were then saved for later analysis. Then subjects moved on to the next condition. Each run lasted 128 s, but only the last 120 s were used for analysis, the first 8 s were used as run-in time. Breaks of around 15 minutes were scheduled after completion of each two conditions, yielding a total time per session of approximately 4 hours, depending on the amount of training required.

C. Data Analysis

The use of two multisine forcing functions, see (8), both with 20 input frequencies that are integer multiples of the measurement base frequency (ω_b=$2\pi/120$ rad/s), facilitates the following frequency-domain analysis.

1) Tracking Performance: The variance of the error σ_e^2 was used as measure of tracking performance. The variance was calculated per measurement run in the frequency domain by integrating the power spectral density function [28]. The contribution of the target and disturbance signals to the error variance were obtained by integrating only over the respective forcing function input frequencies, while the remainder was considered to be due to remnant. Hereby, we neglected the small remnant contribution at the input frequencies.

2) HC Dynamics Estimation: First, frequency responses of $H_{o_t}(j\omega_i)$ and $H_{o_x}(j\omega_i)$ in Fig. 2 were estimated, at the input frequencies ω_i of the target and disturbance signals. An instrumental-variable multiloop system identification technique was used, based on Fourier coefficients [20], [30]. The same method was used to derive the preview tracking model, see [19], [20] for a complete derivation.

Second, following the same procedure as in [19], the model parameter vector Θ was estimated by minimizing a least-squares criterion based on the modeling error ε:

$$\hat{\Theta} = \underset{\Theta}{\operatorname{argmin}} \sum_{i=1}^{40} |\varepsilon(j\omega_i|\Theta)|^2, \tag{9}$$

$$\text{where:} \qquad \varepsilon(j\omega_i|\Theta) = U(j\omega_i) - \hat{U}(j\omega_i|\Theta). \tag{10}$$

$U(j\omega_i)$ is the measured control output, averaged over the five measurement runs in the frequency domain. The modeled control output $\hat{U}(j\omega_i|\Theta)$ is obtained from open-loop simulations of the model in Fig. 2, that is, $\hat{U}(j\omega_i|\Theta) = \hat{H}_{o_t}(j\omega_i|\Theta)F_t(j\omega_i) - \hat{H}_{o_x}(j\omega_i|\Theta)X(j\omega_i)$. To minimize (9) a Nelder-Mead simplex algorithm was used, constrained only to avoid solutions with negative parameters. The best estimate of Θ (given by the lowest criterion value) was selected from 100 randomly initialized optimization runs. In a few cases, when the best solution yielded clear outliers in the parameters, the second best solution was manually selected.

The Variance Accounted For (VAF) was used as measure for the model's quality-of-fit: VAF $= \left[1 - (\sigma_\varepsilon^2/\sigma_u^2)\right] \times 100\%$ [31]. A VAF of 100% reflects that the modeling error ε is zero and that model perfectly describes the measurements.

3) Perfect Target-Tracking: HCs track the target perfectly when $X(j\omega)/F_t(j\omega)$=1. This condition is satisfied when the target frequency response (H_{o_t} in Fig. 2) equals the "perfect" target response $H_{o_t}^P(j\omega) = H_{o_x}(j\omega) + 1/H_{ce}(j\omega)$, see [14] for a detailed derivation. We calculated $H_{o_t}^P(j\omega_i)$ based on the nonparametric frequency response estimate of $H_{o_x}(j\omega_i)$.

V. Experimental Validation: Results

A. Nonparametric Results

1) Tracking Performance: Fig. 4 shows that the measured tracking performance improves when more preview becomes available, both in SI and DI tasks. Performance improves mainly at the target frequencies, although the remnant frequencies also contribute slightly (especially in DI tasks); differences at the disturbance input frequencies are small, which corresponds to [14]. Remarkably, in DI tasks, a minor performance degradation is observed when τ_p is increased from 1.66 to 2 s. Possibly, the additional information distracts the HC or evokes a reduced-effort control strategy. Fig. 4 shows that subjects attain most of the total performance improvement already with only 0.5-0.75 s (SI) and 1-1.66 s (DI) of preview.

In SI tasks, the experimental performance at target and disturbance frequencies matches the RMP almost perfectly. In DI tasks, the RMP consistently predicts superior performance than measured experimentally. Likely, the lack of damping in the CE led to increased remnant and a less linear response (see also [14], [19]), resulting in suboptimal performance.

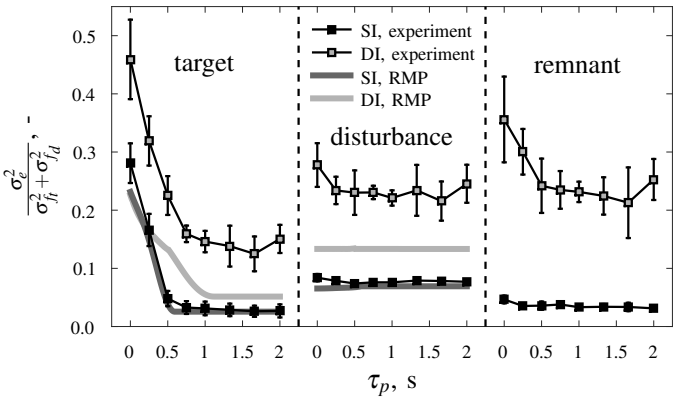

Fig. 4. Experimental tracking error variance, separated into contributions at the target, disturbance, and remnant frequencies; average over eight subjects and 95% confidence intervals, corrected for between-subject variability. The offline model predictions (RMP) are also shown for comparison.

Nonetheless, the exponential trend of improving performance with increasing preview time is almost identical in the RMP and the experiment, and the predicted critical preview times (0.6 s for SI and 1.15 s for DI) are in the same range where the experimental performance stabilizes.

2) Target Response Dynamics: Fig. 5 shows estimates of the HCs' target frequency response function $H_{o_t}(j\omega)$. In both SI and DI tasks, longer preview times yield markedly more phase lead in $H_{o_t}(j\omega)$, which thereby better matches the response required for perfect target-tracking $H_{o_t}^P(j\omega)$ (solid gray line). When the preview time exceeds 0.5 and 0.75 s in SI and DI tasks, respectively, $H_{o_t}(j\omega)$ approximates $H_{o_t}^P(j\omega)$ up to frequencies around 4 rad/s, which is well above the target signal bandwidth (1.5 rad/s). As such, all low-frequency, high-amplitude sinusoids are tracked well and the target-tracking performance improvement saturates with higher preview times, see Fig. 4. In DI tasks, more preview additionally evokes a decreased magnitude of $H_{o_t}(j\omega)$ at higher frequencies, corresponding to the predicted increase of the low-pass filter time constant (see Fig. 3).

Whereas the frequency response estimates are a smooth function of frequency in SI tasks, the estimates in DI tasks are more variable. This is supported by the standard errors of the frequency response estimates in Fig. 6, and is a consequence of both the larger remnant (see Fig. 4), and a general ignorance to track the higher frequencies of the target signal in DI tasks.

Fig. 6 also shows the dynamics predicted by the offline model optimization. Overall, the experiment data matches the predictions reasonably well, although neither RMP nor FMP match the data perfectly. In SI tasks, the measured magnitude peak at the higher frequencies is higher than the RMP, but below the FMP, which suggests that at least several subjects initiated a near-viewpoint response. In DI tasks, the measurements match best with the FMP, both in phase and magnitude, but the difference between RMP and FMP is small. Fig. 6 also reveals some low-frequency lag in the measurements for SI tasks, which are not captured by the predictions; such lag been observed before in preview tracking [19], [22], but is not explicitly included in the model here for simplicity.

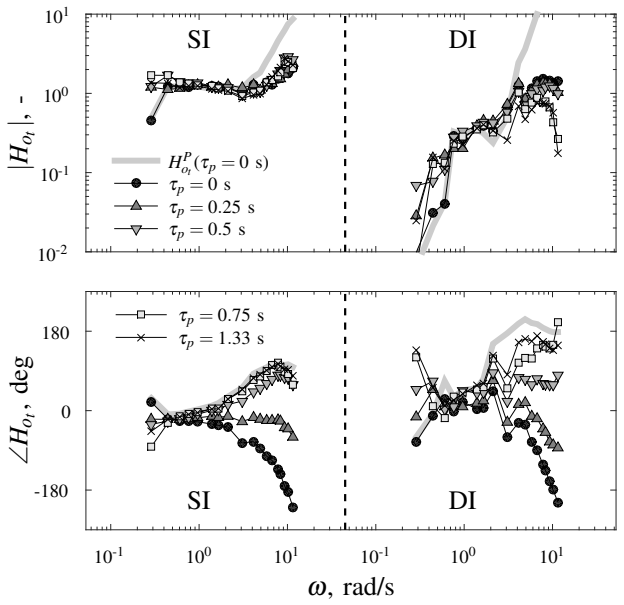

Fig. 5. Frequency response estimates of the experimental target response dynamics (average of all subjects). $H_{o_t}^P(j\omega)$ is only shown for τ_p=0 s, as it is identical at all preview times due to invariance of $H_{o_x}(j\omega)$ (not shown).

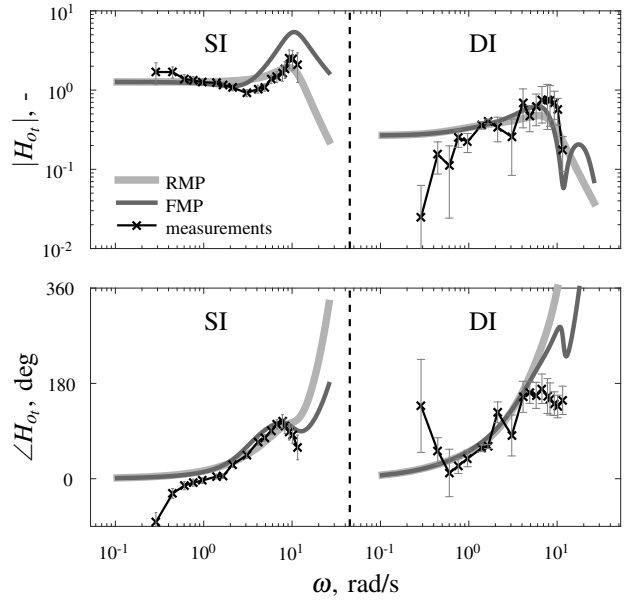

Fig. 6. Comparison of experimental and predicted target response dynamics for τ_p=0.75 s (SI tasks) and τ_p=1.33 s (DI tasks). Measurements indicate the average over the eight subjects and standard error.

B. Modeling Results

1) Variance Accounted For: Both RM and FM fits yield average VAFs well above 85% in SI tasks, and well above 75% in DI tasks (see Fig. 7). The VAF in DI tasks is lower than in SI tasks because of a larger remnant contribution (see Fig. 4), which is not captured by the linear model. The FM provides a consistently higher VAF than the RM, but at the cost of two additional model parameters (K_n and τ_n). With increasing τ_p the improvement in VAF from RM to FM increases, indicating a stronger near-viewpoint response. With short preview times,

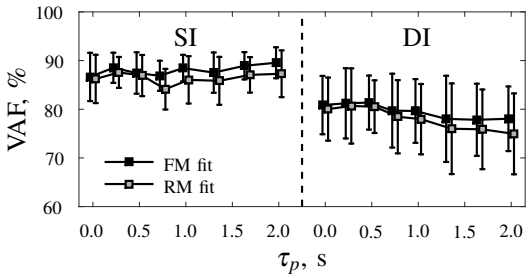

Fig. 7. Average model VAFs, errorbars indicate the standard deviation.

below 0.5 s for SI dynamics and 0.75 s for DI dynamics, the RM and FM describe the data equally well. Therefore, we will not further consider the FM fit results (nor the FMP) at these lower preview times in the remainder of this paper.

2) RM Fits – Internal-Error Response and Physical Limitations: Fig. 8 shows the model's (RM) estimated feedback parameters. In SI tasks, the experimental error response gain $K_{e^\star}$ is approximately invariant, while a 25% decrease was predicted below the critical preview time. The response time delay τ_v decreases from around 0.3 to 0.2 s. In DI tasks, $K_{e^\star}$ increases from 0.15 to 0.28, and while the response delay decreases only slightly, substantially less lead is generated ($T_{L,e^\star}$ drops from 2.7 to 1.5 s). These trends suggest that longer preview times evoke a more aggressive (higher gain) internal-error response at low frequencies, which corresponds to Fig. 5. The neuromuscular break frequency ω_{nms} is in general invariant with preview time, but the damping ratio ζ_{nms} decreases approximately 20-30%.

3) RM Fits – Far-Viewpoint Response: In Fig. 9, the black markers show the estimated far-viewpoint parameters and the gray solid line represents the RMP; these match almost perfectly, especially in SI tasks. As predicted, below the critical preview time, subjects position their far-viewpoint as far ahead as possible ($\tau_f \approx \tau_p$), see Fig. 9a. Although we estimated the model parameters without applying constraints, τ_f is always estimated lower than the preview time (gray shaded area in Fig. 9a), or only slightly higher. As such, τ_f indeed appears to accurately reflect the farthest point along the previewed trajectory ahead that subjects use for control.

When the preview time is above 0.75 s (SI) and 1 s (DI) the experimental τ_f data stabilize. Some subjects (presented with markers in Fig. 9) select a far viewpoint near τ_p even beyond the critical preview time, which was also reported in [7] for a SI task. However, with the highest preview time of 2 s all but one subject (in the DI task) set their τ_f close to the predicted values. Slightly more preview than the critical preview time thus induces HCs to position their far viewpoint at the visually salient endpoint of the winding preview line, opposed to the "optimal" position. This behavior appears to depend on the display scaling, because subjects focused even more on the trajectory's endpoint while using the smaller preview displays in the experiments in [7], [14].

In DI tasks, the estimated far-viewpoint gain K_f increases with preview time, as predicted (Fig. 9b). However, most subjects adopt a K_f well below the unity value of the RMP

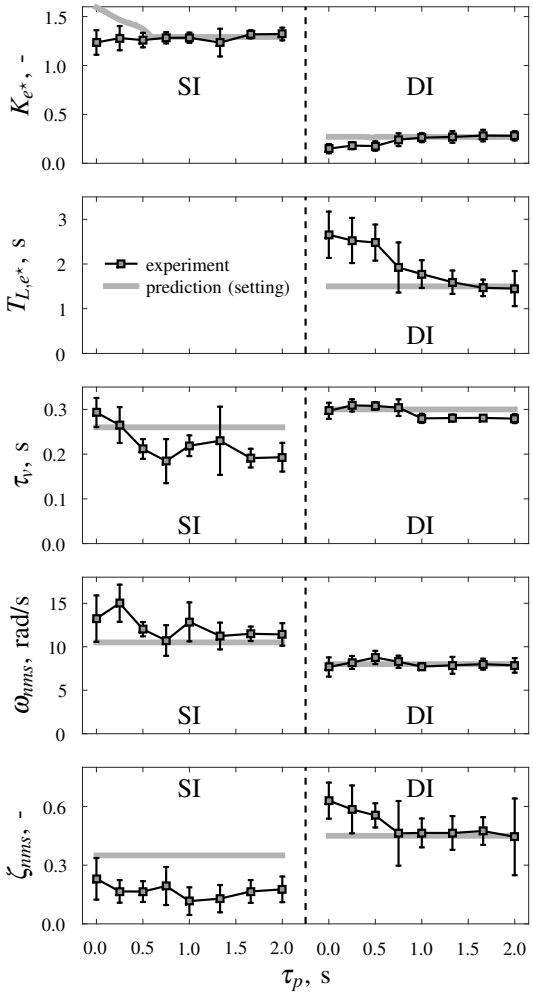

Fig. 8. Internal-error response and physical-limitation parameters obtained from RM fits (FM fits yield similar results), average over eight subjects and 95% confidence intervals, corrected for between-subject variability. The offline predictions are also shown for comparison.

beyond the critical preview time, which explains why the attained tracking performance is worse than predicted (see Fig. 4). In SI tasks, subjects adopt a K_f close to unity, which corresponds to the RMP above the critical preview time. With short preview times the RMP predicted a lower K_f; the difference is approximately 25% for τ_p=0 s, which is equal but opposite to the error in the $K_{e^\star}$ prediction, such that the total target response gain $K_f K_{e^\star}$ was in fact predicted accurately.

The far-viewpoint time constant $T_{l,f}$ (Fig. 9c) increases with preview time, especially in DI tasks, which indicates that subjects respond less to the target's higher frequencies when τ_p increases. Equivalently, a higher $T_{l,f}$ suggests that subjects use a longer region of the target signal for smoothing, which is indeed facilitated by the visible preview. Fig. 9c shows that, as expected, $T_{l,f}$ is typically smaller than τ_p. In SI tasks, the measured $T_{l,f}$ values around 0.1 s imply a break frequency of approximately 10 rad/s, which is near the highest forcing function excitation frequency; the effect of the estimated filter on the model output is thus small. This corresponds roughly with the RMP, which predicts that $T_{l,f} \approx 0$ s. In DI tasks, a higher $T_{l,f}$ was expected from the RMP. Likely, for the less

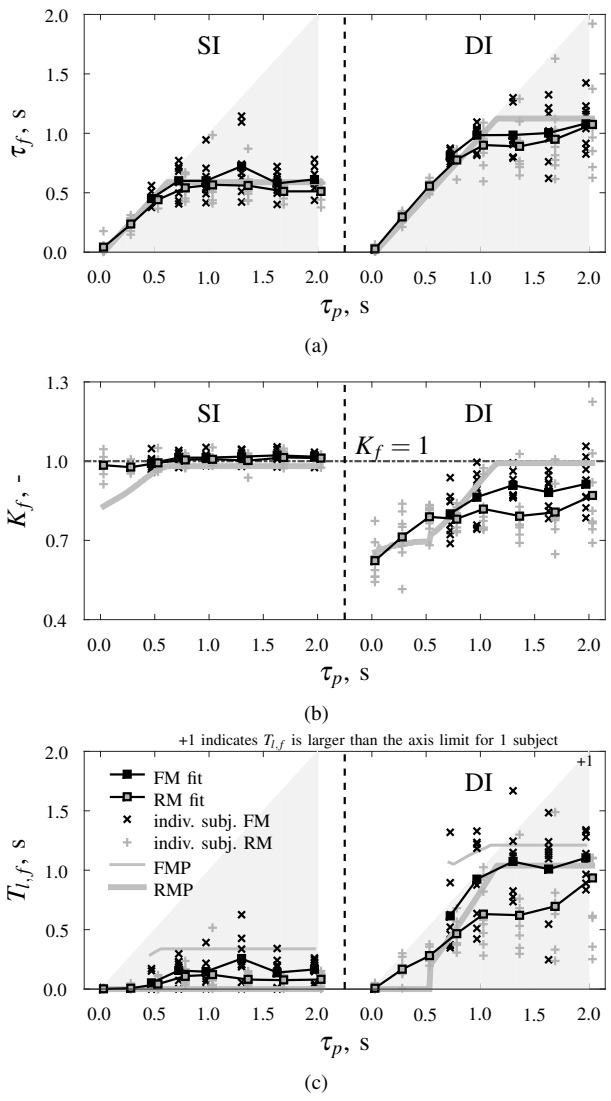

Fig. 9. Estimated far-viewpoint parameters (means and individual subjects) compared to the predictions. Different results are slightly shifted horizontally to prevent overlapping. FM fits (and predictions) are omitted for low preview times because their VAFs are similar to the RM fits.

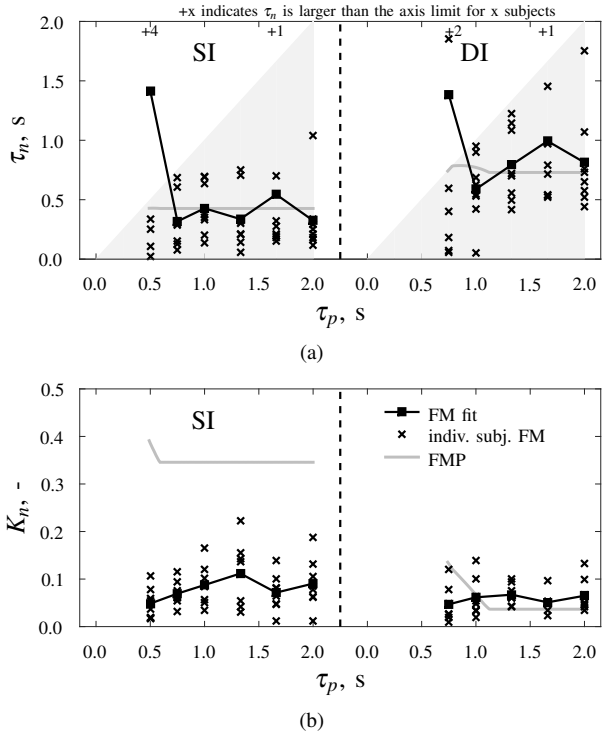

Fig. 10. Estimated near-viewpoint parameters (means and individual subjects) compared to the predictions. Results for low preview times are omitted, because the VAFs of the RM and FM fits are very similar here.

aggressive target response gain K_f adopted by the subjects relative to our model predictions, it is rewarding to attenuate less of the high frequencies with the low-pass filter.

4) FM Fits: Fig. 9 also shows the far-viewpoint parameters estimated with the FM, while Fig. 10 shows the two additional near-viewpoint parameters. Estimated values for τ_f and K_f differ only marginally between RM and FM fits and the trend with changes in preview time is identical. $T_{l,f}$ is in general higher in the FM fit, compared to the RM fit, because the HC's high-frequency target response can be captured by the model's near-viewpoint response.

The near-viewpoint position (τ_n, Fig. 10a) is occasionally estimated to be far beyond the shown preview (i.e., $\tau_n \gg \tau_p$). Such physically impossible values of τ_n occur when no near-viewpoint response is in fact present, as this effectively makes τ_n a free, and ineffectual, parameter. Disregarding the estimates well beyond the preview time limit, τ_n is approximately invariant with preview time, and stabilizes on average around the predicted values of 0.4 and 0.7 s in SI and DI tasks, respectively. Substantial between-subject differences are, however, visible: while most subjects select a near viewpoint that is clearly closer ahead on the previewed target than the far viewpoint, several other subjects select their two viewpoints very close together (i.e., $\tau_n \approx \tau_f$), which suggests that these subjects in fact apply a single-viewpoint control strategy.

The experimental near-viewpoint response gains K_n (Fig. 10b) are also approximately constant above the critical preview time. Clearly, the FMP predicted a much higher K_n compared to the experimental measurements, especially in SI tasks and at lower preview times. This corresponds to results in [14], where it was also shown that a higher value of K_n yields improved performance, but also increased control activity. It thus appears that our subjects also aimed for limited control effort, and not just optimal performance, as was assumed in our offline predictions.

VI. Discussion

The goal of this paper was to quantify and model human control adaptation to variations in available preview time, between 0 and 2 s. To this end, we used the preview tracking model from [19] both to make offline predictions and to analyze measurements from a human-in-the-loop experiment.

Corresponding to previous results [2]–[11] we found evidence supporting our first hypothesis that, below the critical preview time, HCs adapt their control behavior with increasing preview to improve tracking performance. HCs reposition their far viewpoint to the endpoint of the previewed target (i.e., $\tau_f \approx \tau_p$). Moreover, especially in DI tasks, HCs respond more

aggressively to the target (higher K_f) with more preview, while using the longer preview span to better smooth the target signal (higher $T_{l,f}$), effectively ignoring more of the high frequencies.

Just below the critical preview time, more compelling evidence for the presence of a near-viewpoint response occurs. The FM, which includes the near-viewpoint response, captures the measured HC behavior more accurately than the "far-viewpoint only" RM, and the near viewpoint's position is estimated within the range of visual preview for more subjects (i.e., $\tau_n \leq \tau_p$). HCs initiate a near-viewpoint response only when the preview time exceeds approximately 0.5 s (SI) and 0.75 s (DI), with average τ_n values around 0.2 s (SI) and 0.6 s (DI). The preview time needed for an effective near-viewpoint response approximately equals a full period (0.54 s) of the target signal's highest frequency component ($\omega_t = 11.57$ rad/s). This suggests that the near-viewpoint response is in fact not a response to a single point ahead, but to a full sinusoid that is recognized from the target signal. When initiated, the near-viewpoint dynamics are mostly invariant with preview time.

Our second hypothesis was that HC behavior and tracking performance are invariant beyond the critical preview time. This was generally confirmed, but with two caveats. First, several subjects need markedly more preview than the critical preview time to move their far viewpoint away from the endpoint. Second, in DI tasks, tracking performance degraded slightly when the preview time increased from 1.66 s to 2 s. However, no consistent, explanatory adaptation of behavior (i.e., model parameters) was found, so more measurements are required to establish whether the additional preview distracts HCs, evokes a subtle adaptation to a lower effort control strategy, or is an artifact of our modest sample size.

The critical preview time, the transition from adaptive to invariant HC behavior (and performance), was measured to be 0.5-0.75 s (SI) and 1-1.66 s (DI). This is in the same range as the 0.6 s (SI) and 1.15 s (DI) predicted offline, confirming our third hypothesis. Note that these values are not universal: the perfect target tracking dynamics $H_{o_t}^P(j\omega)$ reveal that the critical preview time depends not only on the CE dynamics, but also on the HC's feedback response. For example, a high (feedback) gain $K_{e^\star}$ leads to a lower critical preview time because the CE output intercepts the target signal faster. This lack of critical preview time invariance corresponds to measurements in previous preview tracking experiments [3]–[7], and driving tasks [8], [11].

Compared to similar preview tracking experiments [7], [14], our subjects on average displayed more skilled, proficient manual control behavior, including better tracking performance, a lower response delay τ_v and a higher control gain $K_{e^\star}$. Possible causes include that our subjects performed more tracking runs (eight conditions per CE) and that the experimental preview display was slightly larger compared to [7], [14], which are both known to allow for superior performance. While the presented performance and critical preview times may not be representative for a general population (our subjects were eight relatively young males) and for other tasks, the observed low-level control adaptations to preview time are generalizable, and can be predicted offline for other populations and tasks using the preview model from Fig. 1, see Section III.

The ultimate goal of our work is to obtain a full quantitative understanding of HC manual control behavior and adaptation in general control tasks with preview (e.g., driving). Here, we have established the effects of preview time in tracking task, while previous work has quantified the effects of CE dynamics [14] and the viewing perspective [22]. Other key variables that may trigger human adaptation, but which effects are still poorly understood, are the target signal bandwidth, availability of additional feedback cues (e.g., from vehicle rotations, optic flow, or physical motion), and available lane width (i.e., boundary-avoidance, opposed to our line-tracking task). We intend to quantify human adaptation to these elements in future work, to eventually facilitate predictions and evaluation of HC behavior in a broad range preview control.

VII. Conclusion

This paper investigated the effect of preview time in manual tracking tasks, using a combination of offline model predictions and human-in-the-loop measurements. Increasing the preview time results in better tracking performance, and larger "look-ahead" time model parameters, indicating that subjects respond to a part of the previewed trajectory farther ahead. Beyond a certain "critical" preview time, both tracking performance and control behavior stabilize, and effects of additional preview are small. The critical preview time is not invariant; in tasks with single- and double-integrator controlled element dynamics humans use around 0.6 and 1.15 s of preview, respectively. Measured control adaptations were predicted accurately with the quasi-linear manual control modeling framework. This approach promises to provide insight into human performance limitations due to restricted preview, including the critical preview time, also in other control tasks.

References

[1] R. A. Hess and A. Modjtahedzadeh, "A preview control model of driver steering behavior," in *Proc. 1989 IEEE Int. Conf. Systems, Man, and Cybernetics*, Cambridge, MA, 1989, pp. 504–509.

[2] T. B. Sheridan, "Three models of preview control," *IEEE Trans. Human Factors in Electronics*, vol. 7, no. 2, pp. 91–102, Jun. 1966.

[3] L. D. Reid and N. H. Drewell, "A pilot model for tracking with preview," in *Proc. 8th Ann. Conf. Manual Control*, Ann Arbor, MI, 1972, pp. 191–204.

[4] K. Ito and M. Ito, "Tracking behavior of human operators in preview control systems," *Electrical Eng. in Japan*, vol. 95, no. 1, pp. 120–127, 1975, (Transl,: D.K. Ronbunshi, Vol. 95C, No. 2, Feb. 1975, pp 30-36).

[5] M. Tomizuka and D. E. Whitney, "The preview control problem with application to man-machine system analysis," in *Proc. 9th Ann. Conf. Manual Control*, Cambridge, MA, 1973, pp. 429–441.

[6] A. van Lunteren, "Identification of human operator describing function models with one or two inputs in closed loop systems," Ph.D. dissertation, Mech. Eng., TU Delft, Delft, The Netherlands, 1979.

[7] K. van der El, S. Barendswaard, D. M. Pool, and M. Mulder, "Effects of preview time on human control behavior in rate tracking tasks," in *Proc. 13th IFAC/IFIP/IFORS/IEA Symposium on Analysis, Design and Evaluation of Man-Machine Systems*, Kyoto, Japan, 2016.

[8] J. R. McLean and E. R. Hoffmann, "The effects of restricted preview on driver steering control and performance," *Human Factors*, vol. 15, no. 4, pp. 421–430, 1973.

[9] W. W. Wierwille, J. R. Knight, and G. A. Gagne, "An experimental study of human operator models and closed-loop analysis methods for high-speed automobile driving," *IEEE Trans. Human Factors in Electronics*, vol. 8, no. 3, pp. 187–201, Sep. 1967.

[10] R. A. Hess, "Pursuit tracking and higher levels of skill development in the human pilot," *IEEE Trans. on Systems, Man, and Cybernetics*, vol. 11, no. 4, pp. 262–273, Apr. 1981.

[11] M. F. Land and J. Horwood, "Which parts of the road guide steering?" *Nature*, vol. 377, pp. 339 – 340, Sep. 1995.

[12] D. T. McRuer and H. R. Jex, "A review of quasi-linear pilot models," *IEEE Trans. Human Factors in Electronics*, vol. 8, no. 3, pp. 231–249, May 1967.

[13] M. Mulder, D. M. Pool, D. A. Abbink, E. R. Boer, P. M. T. Zaal, F. M. Drop, K. van der El, and M. M. van Paassen, "Manual control cybernetics: State-of-the-art and current trends," *IEEE Trans. on Human-Machine Systems*, 2017, online preprint available.

[14] K. van der El, D. M. Pool, M. M. van Paassen, and M. Mulder, "Effects of preview on human control behavior in tracking tasks with various controlled elements," *IEEE Trans. on Cybernetics*, vol. 48, no. 4, pp. 1242–1252, Apr. 2018.

[15] D. T. McRuer, D. H. Weir, H. R. Jex, R. E. Magdaleno, and R. W. Allen, "Measurement of driver-vehicle multiloop response properties with a single disturbance input," *IEEE Trans. on Systems, Man, and Cybernetics*, vol. 5, no. 5, pp. 490–497, Sep. 1975.

[16] C. C. MacAdam, "Application of an optimal preview control for simulation of closed-loop automobile driving," *IEEE Trans. Systems, Man, and Cybernetics*, vol. 11, no. 6, pp. 393–399, Jun. 1981.

[17] C. Sentouh, P. Chevrel, F. Mars, and F. Claveau, "A sensorimotor driver model for steering control," in *Proc. 2009 IEEE Int. Conf. Systems, Man, and Cybernetics*, San Antonio, TX, 2009, pp. 2462–2467.

[18] S. D. Keen and D. J. Cole, "Bias-free identification of a linear model-predictive steering controller from measured driver steering behavior," *IEEE Trans. Systems, Man, and Cybernetics - Part B: Cybernetics*, vol. 42, no. 2, pp. 434–443, Apr. 2012.

[19] K. van der El, D. M. Pool, H. J. Damveld, M. M. van Paassen, and M. Mulder, "An empirical human controller model for preview tracking tasks," *IEEE Trans. on Cybernetics*, vol. 46, no. 11, pp. 2609–2621, Nov. 2016.

[20] R. L. Stapleford, D. T. McRuer, and R. E. Magdaleno, "Pilot describing function measurements in a multiloop task," *IEEE Trans. Human Factors in Electronics*, vol. 8, no. 2, pp. 113–125, Jun. 1967.

[21] D. T. McRuer, D. Graham, E. S. Krendel, and W. J. Reisener, "Human pilot dynamics in compensatory systems, theory models and experiments with controlled element and forcing function variations," Air Force Flight Dynamics Laboratory, Wright-Patterson Air Force Base, OH, Tech. Rep. AFFDL-TR-65-15, 1965.

[22] K. van der El, D. M. Pool, M. M. van Paassen, and M. Mulder, "Effects of linear perspective on human use of preview in manual control," *IEEE Trans. on Human-Machine Systems*, 2017, accepted for publication.

[23] D. T. McRuer, R. E. Magdaleno, and G. P. Moore, "A neuromuscular actuation system model," *IEEE Trans. on Man-Machine Systems*, vol. 9, no. 3, pp. 61–71, Sep. 1968.

[24] V. A. Laurense, D. M. Pool, H. J. Damveld, M. M. van Paassen, and M. Mulder, "Effects of controlled element dynamics on human feedforward behavior in ramp-tracking tasks," *IEEE Trans. on Cybernetics*, vol. 45, no. 2, pp. 253–265, Feb. 2015.

[25] F. M. Drop, D. M. Pool, M. M. van Paassen, M. Mulder, and H. H. Bülthoff, "Objective model selection for identifying the human feedforward response in manual control," *IEEE Trans. on Cybernetics*, vol. 48, no. 1, pp. 2–15, Jan. 2018.

[26] R. W. Roig, "A comparison between human operator and optimum linear controller RMS-error performance," *IRE Trans. on Human Factors in Electronics*, vol. 3, no. 1, pp. 18–21, Mar. 1962.

[27] S. Baron and D. L. Kleinman, "The human as an optimal controller and information processor," *IEEE Trans. on Man-Machine Systems*, vol. 10, no. 1, pp. 9–17, Mar. 1969.

[28] H. R. Jex, R. E. Magdaleno, and A. M. Junker, "Roll tracking effects of G-vector tilt and various types of motion washout," in *Proc. 14th Ann. Conf. on Manual Control*, 1978, pp. 463–502.

[29] R. J. Wasicko, D. T. McRuer, and R. E. Magdaleno, "Human pilot dynamic response in single-loop systems with compensatory and pursuit displays," Air Force Flight Dynamics Laboratory, Wright-Patterson Air Force Base, OH, Tech. Rep. AFFDL-TR-66-137, 1966.

[30] M. Olivari, F. M. Nieuwenhuizen, J. Venrooij, H. H. Bülthoff, and L. Pollini, "Methods for multiloop identification of visual and neuromuscular pilot responses," *IEEE Trans. on Cybernetics*, vol. 45, no. 12, Dec. 2015, 2780 - 2791.

[31] J. Venrooij, D. A. Abbink, M. Mulder, M. M. van Paassen, M. Mulder, F. C. T. van der Helm, and H. H. Bülthoff, "A biodynamic feedthrough model based on neuromuscular principles," *IEEE Transactions on Cybernetics*, vol. 44, no. 7, pp. 1141–1154, Jul. 2013.

Kasper van der El (S'15) received the M.Sc. degree in aerospace engineering (*cum laude*) from TU Delft, The Netherlands, in 2013. He is currently pursuing the Ph.D. degree with the section Control and Simulation, Aerospace Engineering, TU Delft, focusing on understanding and modeling human manual control behavior in control tasks with preview. His current research interests include cybernetics, mathematical modeling, and system identification and parameter estimation.

Sharon Padmos received the M.Sc. degree in aerospace engineering from TU Delft, The Netherlands, in 2016, for her research on the effects of preview time on human manual tracking behavior. After her graduation she worked in The Netherlands as a Motion Control Engineer at Ampelmann Operations, as a Software Engineer at Siemens, and, currently, as an Autonomous Systems Scientist at TNO, The Hague.

Daan M. Pool (M'09) received the M.Sc. and Ph.D. degrees (*cum laude*) from TU Delft, The Netherlands, in 2007 and 2012, respectively. He is currently an Assistant Professor with the section Control and Simulation, Aerospace Engineering, TU Delft. His research interests include cybernetics, manual vehicle control, simulator-based training, and mathematical modeling, identification, and optimization techniques.

Marinus (René) M. van Paassen (M'08, SM'15) received the M.Sc. and Ph.D. degrees from TU Delft, The Netherlands, in 1988 and 1994, respectively, for his studies on the role of the neuromuscular system of the pilot's arm in manual control. He is currently an Associate Professor at the section Control and Simulation, Aerospace Engineering, TU Delft. His work on human-machine interaction ranges from studies of perceptual processes and manual control to complex cognitive systems. In the latter field, he applies cognitive systems engineering analysis (abstraction hierarchy and multilevel flow modeling) and ecological interface design to the work domain of vehicle control.

Dr. van Paassen is an Associate Editor of the IEEE TRANSACTIONS ON HUMAN-MACHINE SYSTEMS.

Max Mulder (M'14) received the M.Sc. degree and Ph.D. degree (*cum laude*) in aerospace engineering from TU Delft, The Netherlands, in 1992 and 1999, respectively, for his work on the cybernetics of tunnel-in-the-sky displays. He is currently Full Professor and Head of the section Control and Simulation, Aerospace Engineering, TU Delft. His research interests include cybernetics and its use in modeling human perception and performance, and cognitive systems engineering and its application in the design of "ecological" interfaces.

Prof. Mulder is an Associate Editor of the IEEE TRANSACTIONS ON HUMAN-MACHINE SYSTEMS